IEEE Access
Multidisciplinary | Rapid Review | Open Access Journal

Received April 9, 2020, accepted April 22, 2020, date of publication April 27, 2020, date of current version May 14, 2020.

Digital Object Identifier 10.1109/ACCESS.2020.2990763

An Improved Sliding Mode Control Technique to Mitigate Mismatched Parameter Uncertainties of Three-Phase Voltage Source Inverters

MUHAMMAD SAAD RAFAQ, SADEQ ALI QASEM MOHAMMED, HAN HO CHOI, (Member, IEEE), AND JIN-WOO JUNG, (Member, IEEE)
Division of Electronics and Electrical Engineering, Dongguk University, Seoul 04620, South Korea

Corresponding author: Jin-Woo Jung (jinwjung@dongguk.edu)

This work was supported by the Basic Science Research Program through the National Research Foundation of Korea (NRF) funded by the Ministry of Education under Grant 2018R1D1A1B07046873.

ABSTRACT This paper proposes a theoretical and experimental implementation of an advanced sliding mode control (SMC) for a three-phase voltage source inverter (VSI) to achieve robustness against the unknown uncertainties of an *LC* filter. The significant contributions of the proposed SMC are summarized as considerations for the matched and mismatched uncertainties of the *LC* filter, more relaxed norm-bounds, dynamic characterization of sliding surface, and unique stability analysis. Unlike the conventional SMC techniques with matched uncertainties, the mismatched uncertainties in the state matrix are taken for the design of the proposed SMC. Also, the relaxed norm-bound designed for matched and mismatched uncertainties allows a wide range of variations in the values of *LC* filter. The voltage tracking errors are significantly reduced and the total harmonic distortions (THDs) are highly suppressed by characterizing the sliding surface in terms of flexible linear matrix inequalities (LMIs). Next, the stability analysis and reachability conditions are given using the Lyapunov criterion. The authenticity of the proposed SMC method is proved by TMS320LF28335 DSP based experimental results with a prototype 1-kVA test-bed. The comparative experimental results and analysis for the proposed SMC scheme, the conventional SMC scheme, and the conventional PI−PI control scheme are presented under the load step change, unbalanced load, and non-linear load step change with the parameter uncertainties to demonstrate the excellent performance of the proposed controller such as fast transient response, small steady-state error, and low THD.

INDEX TERMS Parameter uncertainties, sliding mode control (SMC), three-phase voltage source inverter (VSI), total harmonic distortion (THD).

I. INTRODUCTION

Three-phase voltage source inverter (VSI) is the most significant dc-ac component of many advanced applications such as uninterruptable power supplies, renewable energy systems, and active harmonic filters [1]. These applications require constant frequency and constant amplitude with sinusoidal voltage and low high-order harmonic components [2], whereas the quality of the inverter output voltage is seriously affected by sudden load changes, unbalanced loads, and non-linear loads [3]. In order to rectify the distortions and frequency-related switching voltage harmonics in the output voltage, the *LC* filter is connected to the output terminals of the VSI [4]. However, the parameter uncertainties associated with the *LC* filter due to aging and changing operating conditions complicate the control design [5] and stability analysis of the VSI. Also, the changes in the capacitance and inductance of an *LC* filter deteriorate the sinusoidal output voltage. Therefore, over the past few decades, considerable researches [6]–[12] have been done on the voltage control techniques to achieve a fast dynamic response [6], robustness to parameter variations, zero tracking error, and low total harmonic distortion (THD) [7].

The conventional linear proportional-integral (PI) control [8] is easy to implement but its poor capability to tolerate the effects of the parameter variations may deteriorate the control performance. Also, in spite of the extensive gain tuning, it has degraded the transient performance due to the

The associate editor coordinating the review of this manuscript and approving it for publication was Jun Hu.

trade-off between maintaining the system stability over the whole operating range and acquiring the adequate dynamic response during the transients. The linear quadratic regulator (LQR) [9] is presented to compensate for the parameter uncertainties for the VSI, which tunes the gains by selecting the entries of the weighting matrix. However, choosing a good set of values is very time-consuming. The model predictive control (MPC) [10] utilizes a system model at each sampling time to predict the output voltage for each potential switching state and the selection of the switching state criterion is established by the cost function. However, the MPC [11] requires the knowledge of model parameters and does not provide the analysis on stability and robustness. The multivariable feedback linearization control (FLC) [12] considers the non-linearity of a system to achieve a low THD under a non-linear load, but it has a computational complexity. The deadbeat control [13] has also gained attention as it provides the fast transient response by placing all the closed-loop poles at zero and the tracking error settles to zero within few sampling times. However, it is very sensitive to model uncertainties, parameters mismatches, and measurement noise especially for high sampling frequencies. In [14], the adaptive control with compensating terms is used to reduce the computational burden for the VSI, but it has a risk of divergence if the controller gains are not selected properly.

Meanwhile, the sliding mode control (SMC) is a non-linear control method applied in the VSI [15] due to its good dynamic response, robustness, and effective regulation properties in a wide range of operating conditions. Also, the SMC based VSI requires the switching control law and dynamic characterization of the sliding surface to ensure efficient voltage regulation and minimize the steady-state errors under all operating conditions. In [16], a switching control law is utilized in the SMC to drive the VSI uncertainties onto the sliding surface and maintain its trajectory on the sliding surface for all subsequent times. However, the voltage tracking error is not significantly reduced in the transient and steady-state operations. In order to minimize the steady-state errors, the integral term is added in the SMC, i.e., integral SMC (ISMC) for the dc-dc converters [17] and the dc-ac VSI [18], but it does not completely eliminate the voltage tracking errors and high-order harmonics. Meanwhile, the multi-resonant SMC (MRSMC) [19] employs multiple resonant terms in the sliding surface to eliminate the voltage tracking errors in the grid-connected VSI applications, but the computation of the resonant terms requires intensive calculations. In [20], the rotating sliding surface based SMC shows a good tracking performance under different load conditions, but the addition of the fuzzy controller to control the time-varying slopes of the SMC increases its complexity. In [21], the bounded norms for the parameter uncertainties are very strict, which provide insufficient robustness against the parameter uncertainties. Moreover, the conventional SMC techniques do not provide the stabilizing control laws that can suppress the mismatched uncertainties (i.e., uncertainties in the state model that do not satisfy matching conditions).

To accomplish fast transient response, small steady-state error (SSE), insensitivity to mismatched parameter variations, and low THD under critical load conditions, this paper proposes an advanced voltage control law for a three-phase VSI with an *LC* filter based on sliding mode control (SMC). The main contributions of the proposed SMC are summarized as considerations for the matched and mismatched uncertainties of the *LC* filter, more relaxed norm-bounds, dynamic characterization of sliding surface, switching control law, and unique stability analysis. First, both the matched and mismatched uncertainties of an *LC* filter are taken into account in the design of the proposed SMC. Second, the robust SMC law over a wide range of variations in the values of an *LC* filter is achieved by setting the relaxed norm-bounds for these matched and mismatched uncertainties. Third, the SMC design algorithm along with the characterization of the sliding surface and the sufficient condition for the existence of linear sliding surface is presented in terms of linear matrix inequalities (LMIs). Fourth, the switching control law contains a feedforward term, which rejects the disturbances of the VSI. Also, the switching control law drives the VSI trajectories to the sliding surface, and the sliding mode current observer is utilized to estimate the load currents. Fifth, the Lyapunov criterion is utilized to evaluate the stability of the sliding mode dynamics and the reachability conditions of the proposed SMC. Finally, the effectiveness of the proposed sliding mode voltage controller is verified by the experiment results via a prototype 1-kVA VSI test-bed having TMS320LF28335 DSP. The comparative and quantitative experimental results for the proposed SMC scheme, the conventional SMC scheme, and the conventional PI−PI control scheme are presented to prove fast transient response, small steady-state error (SSE), and low THD under load step change, unbalanced load, and non-linear load step change with the parameter uncertainties.

II. DYNAMIC MODEL OF A THREE-PHASE INVERTER

This section describes a dynamic model of the three-phase voltage source inverter (VSI) along with the mismatched parameter uncertainties. Fig. 1 shows the circuit topology of a three-phase inverter with an *LC* filter which consists of a dc-link voltage (V_{dc}), a three-phase pulse-width modulation (PWM) inverter (S_1 to S_6), an output *LC* filter (L_f and C_f),

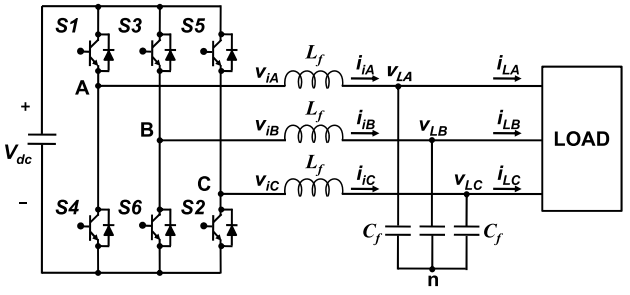

FIGURE 1. Circuit topology of a three-phase voltage source inverter with an *LC* filter.

and a three-phase load. It is noted that the *LC* filter is used to provide sinusoidal output voltages to the load by attenuating the switching frequency components of the VSI. The proposed SMC of the VSI is designed in the *dq*-axis synchronous reference frame in which the three-phase AC signals are transformed to the DC or quasi-DC signals by applying the Park's transformation, which can efficiently control the load voltages under very harmonic polluted load currents. The dynamic model of the three-phase inverter in the *dq*-axis synchronous reference frame can be represented below [22]:

$$\begin{aligned}
\dot{v}_{Ld} &= \omega v_{Lq} + (k_1 + \Delta k_1) i_{id} - (k_1 + \Delta k_1) i_{Ld} \\
\dot{v}_{Lq} &= -\omega v_{Ld} + (k_1 + \Delta k_1) i_{iq} - (k_1 + \Delta k_1) i_{Lq} \\
\dot{i}_{id} &= -(k_2 + \Delta k_2) v_{Ld} + \omega i_{Lq} + (k_2 + \Delta k_2) v_{id} \\
\dot{i}_{iq} &= -(k_2 + \Delta k_2) v_{Lq} - \omega i_{Ld} + (k_2 + \Delta k_2) v_{iq} \qquad (1)
\end{aligned}$$

where v_{id}, v_{iq}, i_{id}, and i_{iq} are the *dq*-axis inverter voltages and currents, v_{Ld}, v_{Lq}, i_{Ld}, and i_{Lq} are the *dq*-axis load voltages and currents, ω is the angular frequency ($\omega = 2\pi \cdot f$), f is the fundamental frequency of output voltage or current, $k_1 = 1/C_f$, $k_2 = 1/L_f$, and Δk_1 and Δk_2 are the parameter deviations in k_1 and k_2 due to aging and changing operating conditions [5], respectively.

III. SWITCHING CONTROL LAW DESIGN AGAINST MISMATCHED NORM–BOUNDED *LC* FILTER UNCERTAINTIES

This section presents the sliding surface design and the switching control law design for the proposed SMC. First, the proposed sliding surface is designed using a more relaxed norm-bounds for the matched and mismatched uncertainties of the *LC* filter. Moreover, the proposed sliding surface is dynamically characterized using the linear matrix inequality (LMI). Next, the switching control law is designed to drive the VSI trajectory to the switching surface and maintain a sliding mode condition.

A. SLIDING SURFACE DESIGN

1) RELAXED NORM-BOUNDS FOR MATCHED AND MISMATCHED UNCERTAINTIES

This subsection presents the relaxed norm-bounds for the matched and mismatched uncertainties of *LC* filter that are used to design the proposed sliding surface. According to the control theory, the matched uncertainties lie within the range space of the control input matrix, while the mismatched uncertainties do not lie within the range space of the input matrix. It should be noted that although the matched uncertainties can be easily removed by a properly designed control input, the mismatched uncertainties cannot be completely rejected [23]. Therefore, the design of a stabilizing controller for a mismatched uncertain system is a challenging task. Also, the robust SMC for the wide range variations in the parameter uncertainties of L_f and C_f is achieved by setting the relaxed conditions for the norm-bounds. The design of the mathematical norm-bounds is important so that the SMC can mitigate both matched and mismatched uncertainties. Consequently, the parameter uncertainties Δk_1 and Δk_2, due to aging and changing operating conditions [6], in (1) are norm-bounded with the assumptions that there exist the known finite constants ρ_1, ρ_2 such that $|\Delta k_2| \leq \rho_2 k_2 \ll k_2$; $|\Delta k_1| \leq \rho_1 k_1$, and $(\rho_1 \,/\, (1-\rho_1)) \ll k_1$. These inequalities imply that

$$\left| \frac{1}{k_1} - \frac{1}{k_1 + \Delta k_1} \right| = \left| \frac{\Delta k_1}{k_1 (k_1 + \Delta k_1)} \right| \leq \frac{\rho_1}{(1 - \rho_1) k_1} \approx 0. \qquad (2)$$

And for all the bounded but unknown disturbances with the bounded time derivative uncertainties, there exists a solution which is also uniformly bounded. Hence, by utilizing the relaxed norm-bounds which set very high limits for the parameter variations of L_f and C_f, the proposed SMC will produce the sinusoidal output voltage and ensure the robustness for all the wide range of parameter variations in the L_f and C_f within the limits set by the norm-bounds.

2) DYNAMIC CHARACTERIZATION OF SLIDING SURFACE

In this subsection, the new design of robust sliding surface against the matched and mismatched uncertainties is presented based on the LMI approach by setting the decay rate within the bounds. The reference values i_{d_ref} and i_{q_ref} for i_{id} and i_{iq} are explicitly explained as

$$\begin{aligned}
i_{d_ref} &= i_{Ld} - \frac{1}{k_1 + \Delta k_1} \omega v_{q_ref} \approx i_{Ld} - \frac{1}{k_1} \omega v_{q_ref} \\
i_{q_ref} &= i_{Lq} + \frac{1}{k_1 + \Delta k_1} \omega v_{d_ref} \approx i_{Lq} + \frac{1}{k_1} \omega v_{d_ref}. \qquad (3)
\end{aligned}$$

and v_{d_ref}, v_{q_ref} are the reference values of v_{Ld} and v_{Lq}. It is more convenient to use the error dynamics of the state variables for designing the sliding surface of the VSI as follows:

$$\begin{aligned}
v_{de} &= v_{Ld} - v_{d_ref}, \quad v_{qe} = v_{Lq} - v_{q_ref} \\
i_{de} &= i_{id} - i_{d_ref}, \quad i_{qe} = i_{iq} - i_{q_ref}. \qquad (4)
\end{aligned}$$

The state-space model of the VSI employing the error dynamics is given as

$$\dot{x} = [A + \Delta A] x + B[u_R + d] \qquad (5)$$

where x represents the state variables, u_R represents the reaching switching control law, ΔA symbolizes the mismatched uncertainties, and d represents the disturbance inputs and matched parameter uncertainties,

$$x = \begin{bmatrix} v_{de} \\ v_{qe} \\ i_{de} \\ i_{qe} \end{bmatrix}, \quad A = \begin{bmatrix} 0 & \omega & k_1 & 0 \\ -\omega & 0 & 0 & k_1 \\ 0 & 0 & 0 & 0 \\ 0 & 0 & 0 & 0 \end{bmatrix}, \quad B = \begin{bmatrix} 0 & 0 \\ 0 & 0 \\ k_2 & 0 \\ 0 & k_2 \end{bmatrix},$$

$$u_R = \begin{bmatrix} v_{id} \\ v_{iq} \end{bmatrix},$$

$$d = \begin{bmatrix} d_d \\ d_q \end{bmatrix} = \begin{bmatrix} -v_{Ld} + \frac{1}{k_2} \omega i_{Lq} + \frac{\Delta k_2}{k_2} v_{Ld} + \frac{\Delta k_2}{k_2} v_{id} \\ -v_{Lq} - \frac{1}{k_2} \omega i_{Ld} - \frac{\Delta k_2}{k_2} v_{Lq} + \frac{\Delta k_2}{k_2} v_{iq} \end{bmatrix}.$$

In d (i.e., d_d and d_q), the first and second terms are the disturbance inputs, and the third and fourth terms denote the matched parameter uncertainties. Also, the mismatched uncertainties ΔA are not required to be matched and they can be decomposed as follows:

$$\Delta A = \begin{bmatrix} 0 & 0 & \Delta k_1 & 0 \\ 0 & 0 & 0 & \Delta k_1 \\ 0 & 0 & 0 & 0 \\ 0 & 0 & 0 & 0 \end{bmatrix} = NM\Delta k_1,$$

$$N = \begin{bmatrix} 1 & 0 \\ 0 & 1 \\ 0 & 0 \\ 0 & 0 \end{bmatrix}, \quad M = \begin{bmatrix} 0 & 0 \\ 0 & 0 \\ 1 & 0 \\ 0 & 1 \end{bmatrix}^T.$$

The parameter deviations in the LC filter are the norm bounded uncertainties (2) in the state matrix as well as the input matrix. The sufficient condition for the existence of the sliding surface sliding surface is presented in terms of LMIs by referring to [24]. Then, the sliding surface S is parameterized as

$$\sigma = Sx = (B^T PB)^{-1} B^T P\, x = \begin{bmatrix} \sigma_1 \\ \sigma_2 \end{bmatrix} = 0 \tag{6}$$

where $P = X^{-1} \in R^{4\times 4}$ is a positive-definite matrix satisfying the following LMI condition

$$\begin{bmatrix} \Phi^T(AX + XA^T + NN^T)\Phi & \rho_1 k_1 \Phi^T XM^T \\ \rho_1 k_1 MX\Phi & -I \end{bmatrix} < 0. \tag{7}$$

In the above LMI condition, the symbol $\Phi \in R^{4\times 2}$ denotes the orthogonal complement of B and a full rank matrix such that $\Phi^T B = 0$ and $\Phi^T\Phi = I$. It should be noted that the sliding surface matrix $S \in R^{2\times 4}$ has a null space identical to $B^T P$. In this regard, a transformation matrix T and its associated vector Z are defined as

$$T = \begin{bmatrix} (\Phi^T X\Phi)^{-1}\Phi^T \\ (B^T PB)^{-1}B^T P \end{bmatrix}, \quad Z = Tx = \begin{bmatrix} z \\ \sigma \end{bmatrix}. \tag{8}$$

It is easy to show that $T^{-1} = [X\Phi, B]$. By using the Shur's complement lemma [25], we can show that the LMI condition (7) is equivalent to the following Riccati-like inequality

$$\Phi^T[AX + XA^T + NN^T + (\rho_1 k_1)^2 XM^T MX]\Phi < 0. \tag{9}$$

It should be noted that the result of [25] implies the existence of some positive constant ρ_M guaranteeing the feasibility of the LMI (7) or equivalently (9) for any $0 \le \rho_1 \le \rho_M$.

Remark 1: It is worth noting that the proposed sliding mode control (SMC) guarantees a better voltage control performance such as better robustness against the parameter variations of both L_f and C_f, more relaxed norm-bounds for the wide range variations of an LC filter, and more dynamic LMIs for the characterization of the sliding surface compared to the conventional SMC in [21]. First, the proposed SMC considers the parameter variations of both L_f and C_f, while [21] taking into consideration the parameter variations of L_f only. If the parameter deviation Δk_2 of L_f lies within the range space of the control input matrix B, it is taken as the matched uncertainties. On the other hand, if the parameter deviation Δk_1 of C_f does not lie within the range space of B, it is considered as the mismatched uncertainties. Hence, unlike [21], both the matched and mismatched uncertainties (i.e., Δk_1 and Δk_2) are taken into account to design the proposed SMC law with low THD and small steady-state error in the output voltage. Second, unlike [21], the norm-bounded uncertainties presented in this paper are more relaxed (i.e., the parameters (e.g., L_f and C_f) constrained by the norm-bounds can have a wide range of variations), which enable the robust behavior of the proposed SMC against the wide range uncertainties in L_f and C_f. Last, the proposed SMC employs the LMIs in the form of Riccati like inequalities which are more dynamic with a completely different structure from [21] to characterize the sliding surface, whereas [21] utilizes the Lyapunov inequality to design the sliding surface of the conventional SMC. Consequently, the proposed SMC method can achieve more robustness against the parameter variations, faster dynamic response, and smaller steady-state error in comparison to [21].

B. SWITCHING CONTROL LAW DESIGN

The objective of this subsection is to determine the reaching control law and the switched feedback gains which can drive the VSI trajectory to the switching surface and maintain a sliding mode condition. The variable structure control u_R is designed such that the error dynamics x of the VSI outside the switching surface are driven to reach the sliding surface in finite time. The control variable $u_R = [v_{id}\ v_{iq}]^T$ can be divided into the following two terms

$$u_R = v_{ff} + v_{fb} \tag{10}$$

where $v_{ff} = [v_{ffd} v_{ffq}]^{\mathrm{T}}$ are the feedforward control terms for the compensation of matched disturbance inputs in d given as

$$v_{ff} = \begin{bmatrix} v_{ffd} \\ v_{ffq} \end{bmatrix} = \begin{bmatrix} v_{Ld} \\ v_{Lq} \end{bmatrix} + \frac{1}{k_2}\omega \begin{bmatrix} -i_{Lq} \\ i_{Ld} \end{bmatrix} \tag{11}$$

and $v_{fb} = [v_{fbd}\ v_{fbq}]^{\mathrm{T}}$ are the switching feedback control terms to force the system trajectories to the sliding surface ($\sigma = 0$), presented as

$$v_{fb} = \begin{bmatrix} v_{fbd} \\ v_{fbq} \end{bmatrix} = \begin{bmatrix} -D_d x - \rho_d(t)SIGN(\sigma_1) \\ -D_q x - \rho_q(t)SIGN(\sigma_2) \end{bmatrix} \tag{12}$$

where $SA = [D_d^T D_q^T]^T$ are the matrix product of the sliding surface matrix S and the control state matrix A, and

$$\rho_d(t) = \kappa_d + \frac{1}{1-\rho_2}\begin{bmatrix} \rho_1 k_1 |H_d x| + 2\rho_2 |v_{Ld}| \\ +\frac{\rho_2}{k_2}\omega |i_{Lq}| + \rho_2 |D_d x| \end{bmatrix},$$

$$\rho_q(t) = \kappa_q + \frac{1}{1-\rho_2}\begin{bmatrix} \rho_1 k_1 |H_q x| + 2\rho_2 |v_{Lq}| \\ +\frac{\rho_2}{k_2}\omega |i_{Ld}| + \rho_2 |D_q x| \end{bmatrix}. \tag{13}$$

with $\kappa_d > 0$, $\kappa_q > 0$, and $SNM = [H_d^T H_q^T]^T$.

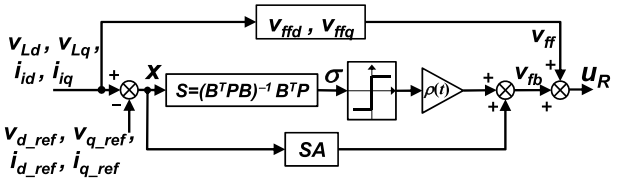

FIGURE 2. Block diagram of the proposed sliding mode control for a VSI.

Fig. 2 presents the block diagram of the proposed sliding mode control for a VSI with S and SA explained in (6) and (12), respectively. In this figure, the small values of $\rho(t)$, i.e., ρ_d and ρ_q are more suitable for the steady-state operating condition. However, in terms of control activities, too small values of ρ_d and ρ_q can lead to slow transient responses. Therefore, the values of ρ_d and ρ_q should satisfy the two state sides, i.e., the steady-state and transient responses.

IV. SLIDING-MODE OBSERVER BASED CONTROL LAW AND STABILITY ANALYSIS

This section presents the sliding mode observer (SMO) that estimates the load currents i_{Ld} and i_{Lq}. Furthermore, the estimated load currents are used by the proposed SMC to design the SMO-based control law. Next, the stability analysis of the proposed SMO-based control law is presented using the Lyapunov function.

A. SLIDING-MODE LOAD CURRENT OBSERVER-BASED CONTROL LAW

To accurately estimate the load currents i_{Ld} and i_{Lq} under the wide range of parameter variations and noisy environments [25], the sliding mode observer (SMO) is employed due to its robustness to the external disturbances. Moreover, the load current SMO omits the situations of sudden breakdown of the current sensors and provides the reliability and cost reduction to the VSI. In this paper, it is assumed that the load currents change slowly during a small sampling period [25]. The sliding mode based load current observer for the i_{Ld} and i_{Lq} is represented as;

$$\begin{aligned}\dot{\hat{v}}_{Ld} &= \omega v_{Lq} + k_1 i_{id} + l_d SIGN\left(v_{Ld} - \hat{v}_{Ld}\right)\\ \dot{\hat{v}}_{Lq} &= \omega v_{Ld} + k_1 i_{iq} + l_q SIGN\left(v_{Lq} - \hat{v}_{Lq}\right)\end{aligned} \tag{14}$$

where $l_d \gg 1$ and $l_q \gg 1$. By referring to [24], [26], [27] and references therein, the error dynamics of the SMO can be derived from (1)

$$i_{Ld} \approx -\frac{l_d}{k_1} SIGN\left(v_{Ld} - \hat{v}_{Ld}\right), \tag{15}$$

$$i_{Lq} \approx -\frac{l_q}{k_1} SIGN\left(v_{Lq} - \hat{v}_{Lq}\right). \tag{16}$$

To estimate the load currents i_{Ld} and i_{Lq} [25], an averaging filter, i.e., a low pass filter is designed such that the characteristics of the signals are determined by the low frequencies and the unmodeled dynamics produces the high frequencies. The estimated load currents can be calculated as;

$$\begin{aligned}\hat{i}_{Ld} &= -\frac{1}{1+\tau_d s}\cdot\frac{l_d}{k_1} SIGN(v_{Ld} - \hat{v}_{Ld})\\ \hat{i}_{Lq} &= -\frac{1}{1+\tau_q s}\cdot\frac{l_q}{k_1} SIGN(v_{Lq} - \hat{v}_{Lq})\end{aligned} \tag{17}$$

where $0 < \tau_d \ll 1, 0 < \tau_q \ll 1$ are small filter time constants and s is the Laplace variable.

These estimated load currents $\hat{i}_{Ld}, \hat{i}_{Lq}$ are utilized for constructing the error dynamics of the estimated state vector $\hat{x} = [v_{de}, v_{qe}, \hat{i}_{de}, \hat{i}_{qe}]^T$ such that

$$\hat{i}_{de} = i_{id} - \hat{i}_{Ld} + \frac{1}{k_1}\omega v_{q\_ref}, \quad \hat{i}_{qe} = i_{iq} - \hat{i}_{Lq} - \frac{1}{k_1}\omega v_{d\_ref}. \tag{18}$$

The SMO-based control law can be rewritten as;

$$\begin{aligned}v_{id} &= v_{Ld} - \frac{1}{k_2}\omega\hat{i}_{Lq} - D_d\hat{x} - \hat{\rho}_d SIGN\left(\hat{\sigma}_1\right)\\ v_{iq} &= v_{Lq} + \frac{1}{k_2}\omega\hat{i}_{Ld} - D_q\hat{x} - \hat{\rho}_q SIGN\left(\hat{\sigma}_2\right)\end{aligned} \tag{19}$$

where $\hat{\rho}_d$ and $\hat{\rho}_q$ are given by

$$\begin{aligned}\hat{\rho}_d(t) &= \kappa_d + \frac{1}{1-\rho_2}\left[\begin{array}{l}\rho_1 k_1\left|H_d\hat{x}\right| + 2\rho_2\left|v_{Ld}\right|\\ \quad + \dfrac{\rho_2}{k_2}\omega\left|\hat{i}_{Lq}\right| + \rho_2\left|D_d\hat{x}\right|\end{array}\right],\\ \hat{\rho}_q(t) &= \kappa_q + \frac{1}{1-\rho_2}\left[\begin{array}{l}\rho_1 k_1\left|H_q\hat{x}\right| + 2\rho_2\left|v_{Lq}\right|\\ \quad + \dfrac{\rho_2}{k_2}\omega\left|\hat{i}_{Ld}\right| + \rho_2\left|D_q\hat{x}\right|\end{array}\right].\end{aligned} \tag{20}$$

Thus, the performance of the VSI will be robust to the measurement noise by utilizing the load currents provided by the SMO.

B. STABILITY ANALYSIS

This subsection discusses the stability of the SMO-based control law by analyzing the sliding mode dynamics and reachability conditions. The estimated state vector $\hat{x} = [v_{de}, v_{qe}, \hat{i}_{de}, \hat{i}_{qe}]^T$ converges to the actual state x, i.e., the SMO-based control law (19) converges to (10). By the separation property given in [24], [26], [27], it is sufficient to show that the sliding mode dynamics with the switching control law (10) are stable and the reachability condition $\sigma^T\dot{\sigma} < 0$ is guaranteed for all $\sigma \neq 0$. First, the stability analysis of the sliding mode dynamics is presented using the Lyapunov function. In this regard, the resulting reduced-order sliding mode dynamics restricted to the switching surface S with the input control law are defined using (8) as follows:

$$z = (\Phi^T X \Phi)^{-1}\Phi^T x \tag{21}$$

where $z \in R^2$. Then, from (5) the sliding mode dynamics are given by the following uncertain second-order equation

$$\dot{z} = \left(\Phi^T X \Phi\right)^{-1}\Phi^T\left[A + \Delta A\right] X \Phi z. \tag{22}$$

The stability of the sliding mode dynamics requires the selection of a generalized Lyapunov function $V(t,z)$ which

is positive definite and has a negative time derivative in the region of attraction. Therefore, the Lyapunov function to yield an appropriate sliding mode for mismatched uncertainties is defined as

$$V(z) = z^T \left(\Phi^T X \Phi\right) z. \tag{23}$$

And its derivative is calculated as

$$\begin{aligned}\dot{V} &= 2z^T \Phi^T \left[A + NM\Delta k_1\right] X \Phi z \\ &\le z^T \Phi^T [AX + XA^T + N^T N + |\Delta k_1|^2 XM^T MX] \Phi z \\ &\le z^T \Phi^T [AX + XA^T + N^T N + (\rho_1 k_1)^2 XM^T MX] \Phi z \\ &\le 0 \end{aligned} \tag{24}$$

where the Riccati-like inequality (9) is used to prove the stability. The time derivative of the above Lyapunov function (24) is negative for all $z \neq 0$, which proves the stability of the sliding mode dynamics (22).

Second, the stability analysis of the reachability condition is presented by highlighting that the sliding motion is reached with the switching feedback control law. The reachability condition is proven for all $\sigma \neq 0$ such that

$$\begin{aligned}\sigma^T \dot{\sigma} &= \sigma^T (SAx + SNM\Delta k_1 x + u_R + d) \\ &= \sigma_1 (D_d x + \Delta k_1 H_d x + v_{id} + d_d) \\ &\quad + \sigma_2 (D_q x + \Delta k_1 H_q x + v_{iq} + d_q) \\ &\le |\sigma_1| \left(\rho_1 k_1 |H_d x| + \rho_2 |v_{Ld}| + \rho_2 |v_{id}| - \rho_d\right) \\ &\quad + |\sigma_2| \left(\rho_1 k_1 |H_q x| + \rho_2 |v_{Lq}| + \rho_2 |v_{iq}| - \rho_q\right) \\ &\le |\sigma_1| \begin{pmatrix} \rho_1 k_1 |H_d x| + \rho_2 |v_{Ld}| \\ + \rho_2 \left[|v_{Ld}| + \frac{1}{k_2}\omega |i_{Lq}| + |D_d x| + \rho_d\right] - \rho_d \end{pmatrix} \\ &\quad + |\sigma_2| \begin{pmatrix} \rho_1 k_1 |H_q x| + \rho_2 |v_{Lq}| + \\ \rho_2 \left[|v_{Lq}| + \frac{1}{k_2}\omega |i_{Ld}| + |D_q x| + \rho_q\right] - \rho_q \end{pmatrix} \\ &\le -\frac{1}{1-\rho_2} \left[\varepsilon_d |\sigma_d| + \varepsilon_q |\sigma_q|\right]. \end{aligned} \tag{25}$$

Hence, the convergence of σ is proven by the Lyapunov stability criteria. Thus, the reachability conditions are guaranteed, and the state-space model (5) with a SMC law is asymptotically stable in spite of the mismatched uncertainties and external disturbances. The physical meaning of the stability analysis and reachability conditions is that the proposed SMC will converge to the solution under all operating conditions. Then, the proof of the stability analysis of the sliding mode dynamics and reachability conditions provides the analytical analysis on a much wider scale compared to the numerical analysis.

Accordingly, the design procedure for the practical implementation of the proposed sliding mode voltage controller can be summarized by the following:

Step 1) Build the system model (1) in d–q coordinate frame, and then derive the error dynamics (4) by using system parameters.

Step 2) Get the estimated load currents $\hat{i}_{Ld}$, $\hat{i}_{Lq}$ from (17) using the observer gain parameters τ_d, τ_q, l_d, and l_q.

Step 3) Determine the solution X using the LMI conditions (7) and (9).

Step 4) Solve the sliding surface parameter matrix σ in (6) using the solution X.

Step 5) Calculate the switching feedback control law (19) using the controller gains ρ_d and ρ_q from (20).

As depicted in Fig. 2, the proposed SMC can be easily implemented by solving S and SA. It is also noted that the tuning of the controller gains ρ_d and ρ_q is simple, so the proposed SMC does not require any exhaustive gain tuning as the gains are calculated from (20).

V. IMPLEMENTATION AND COMPARATIVE PERFORMANCE ANALYSIS UNDER WIDE-RANGE *LC* FILTER UNCERTAINTIES

A. EXPERIMENTAL SETUP

To prove the authenticity and effectiveness of the proposed SMC algorithm, experiments with a prototype 1 kVA testbed are conducted for the following three scenarios, i.e., a load step change from no load to full load, an unbalanced load by suddenly opening one phase, and a non-linear load step change with a full-bridge diode rectifier. Note that these operating scenarios are selected to highlight the robustness of the proposed SMO under parameter variations. In this paper, the conventional SMC scheme [15] is used to carry out the comparative studies with the proposed SMC method. In addition, the conventional PI-PI control scheme is chosen for another comparative study to authenticate the superior performance of the proposed observer-based SMC scheme. Note that the PI gains are tuned using a general tuning rule mentioned in [3]. The optimum values of the control parameters for the proposed SMC are calculated as $\tau_d = 0.0001$, $\tau_q = 0.0001$, $l_d = 60000$, $l_q = 50000$, $\kappa_d = 0.1$, and $\kappa_q = 0.1$ due to the trade-off between the higher values increasing the chattering problem and the lower values reducing the convergence rate. The filter time constants τ_d and τ_q should be sufficiently small to preserve the control input component undistorted and large enough to eliminate the high-frequency components [28]. Meanwhile, the small values of the l_d and l_q can produce a slow convergence of the estimated load current, whereas the large values of the l_d and l_q can induce the chattering problem in the estimated load current values.

Furthermore, the control parameters κ_d and κ_q are the small offset values added in the gains of the SMC control to avoid the zero multiplication condition and execute the experiments. By solving the LMI condition (7), the solution matrix X is obtained and the sliding surface parameter matrix S is derived from (6) as follows:

$$S = \begin{bmatrix} 0.0018 & 0.00007 & 0.0196 & 0.00012 \\ 0.00002 & 0.003 & 0.00045 & 0.0185 \end{bmatrix}. \tag{26}$$

Fig. 3(a)−(c) presents the schematic diagram of the proposed sliding mode voltage control system using a 16-bit floating point TMS320LF28335 DSP, the photograph of the test-bed used to obtain all the experiment results, and the

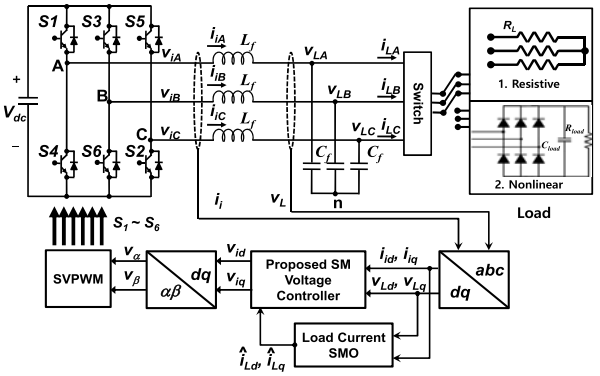

(a)

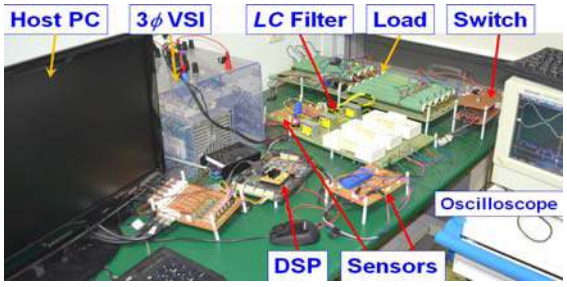

(b)

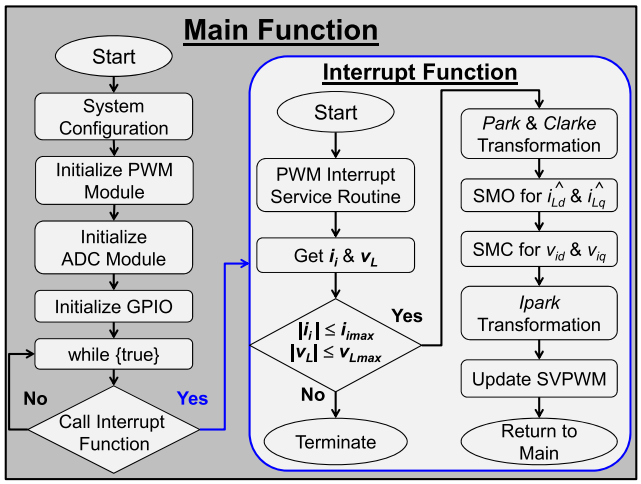

(c)

FIGURE 3. Experimental set-up of the proposed sliding mode control system. (a) Schematic diagram. (b) Photograph of the test-bed. (c) Flowchart of the DSP code.

flowchart of the DSP code to implement the experiments of the proposed SMC, respectively.

As shown in this figure, the load for each operating scenario is selected by the switch. The measured inverter phase currents (i_i) and line-to-neutral load voltages (v_L) in the *abc* reference frame are transformed into the corresponding quantities in the synchronously rotating *d-q* reference frame. Then, these *dq*-axis quantities are provided to the proposed sliding mode voltage controller. The command signals (v_{id} and v_{iq}) are transformed into the quantities (v_α and v_β) in the stationary α-β reference frame to implement a space-vector PWM (SVPWM) technique [29], [30]. In the experiments, the THD, root-mean square (RMS) values, and some waveforms for the experimental results are obtained using a Tektronix digital oscilloscope TDS5000, which is equipped with integrated power measurement and analysis (power analyzer) software. Note that the parameters of the *LC* filter are selected by considering several key factors such as cost, volume, and switching frequency. In the paper, the switching frequency (f_s) is selected as 5 kHz by taking into account a trade-off between the control performance and the efficiency with low switching loss. Even if numerous options of the *L-C* combinations are available for the selected f_s, the capacitance $C_f = 7\ \mu$F is first chosen to minimize the no-load currents in capacitors and capacitor hardware cost, and then the inductance $L_f = 10$ mH is properly selected based on the C_f. In practical applications, the most common tolerance variations of the filter inductance (L_f) and filter capacitance (C_f) used as an output filter are within $\pm 10\%$. To further justify the robustness against parameter variations, $\pm 50\%$ variations in respective L_f and C_f are assumed under all load conditions such as load step change, unbalanced load, and non-linear load step change. It is noted that the parameters of the non-linear load (i.e., $R_{load} = 200\ \Omega$ and $C_{load} = 330\ \mu$F) shown in Fig. 3(a) are selected to achieve the maximum crest factor by considering the overcurrent limitation of our VSI. Table 1 presents the system parameters used to perform the experiments. In the following subsections, the detailed comparative studies with the experimental results will be presented.

TABLE 1. System parameters of a prototype 1 kVA test-bed.

Parameters	Descriptions	Values	Units
L_{f0}	Output filter inductance	10	[mH]
C_{f0}	Output filter capacitance	7	[μF]
R_L	Resistance for linear load	60	[Ω]
R_{load}	Resistance for nonlinear load	200	[Ω]
C_{load}	Capacitance for nonlinear load	330	[μF]
V_{dc}	dc-link voltage	295	[V]
T_s	Sampling time	200	[μs]
f_s	Switching frequency	5	[kHz]
f_1	Fundamental frequency	60	[Hz]
$V_{L,\,rms}$	Load output voltage	110	[V]

B. COMPARATIVE PERFORMANCE ANALYSIS UNDER A SUDDEN LOAD STEP CHANGE WITH WIDE-RANGE LC FILTER UNCERTAINTIES (i.e., 150% L_{f0} AND 50% C_{f0})

To highlight the effectiveness and robustness of the proposed SMC against matched and mismatched uncertainties, the experiments are conducted with wide range variations of L_f and C_f. In this scenario, the variations in the values of the *LC* filter are selected as 150% L_{f0} (i.e., $L_f = 1.5 \times L_{f0}$) and 50% C_{f0} (i.e., $C_f = 0.5 \times C_{f0}$) to verify the robustness of the proposed SMC. Hence, the proposed SMC can effectively regulate the voltage with wide range variations of an *LC* filter. Fig. 4(a)−(b) shows the experimental results of the proposed SMC and the conventional SMC with the waveforms of v_L, i_L,

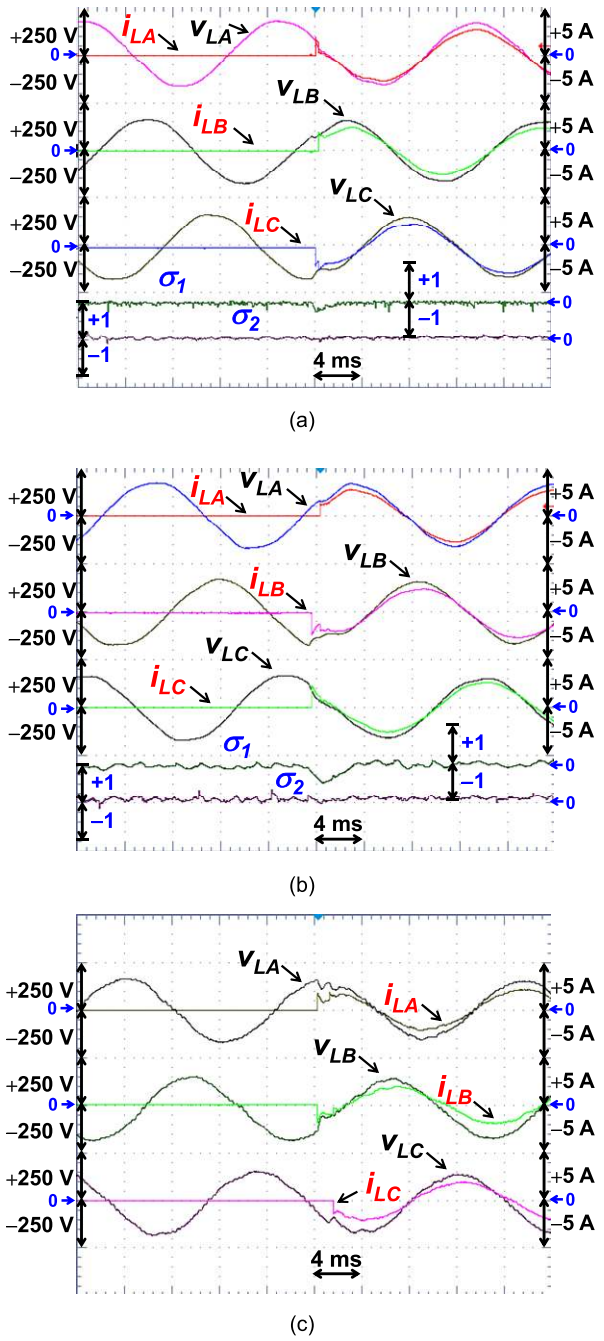

FIGURE 4. Experimental waveforms (v_L, i_L, σ_1, and σ_2) under a sudden load step change (i.e., resistive load: 0% to 100%) with $L_f = 150\%\ L_{f0}$ and $C_f = 50\%\ C_{f0}$. (a) Proposed observer-based SMC scheme. (b) Conventional observer-based SMC scheme. (c) Conventional PI−PI control scheme.

σ_1, and σ_2, while Fig. 4(c) shows the experimental results of the conventional PI−PI control scheme with the waveforms of v_L and i_L under the scenario of a sudden load step change. In Fig. 4(a), the load output voltages are restored within less than only half a cycle after the load is suddenly applied. Even though the v_L slightly exhibits the undershoot due to the underdamped nature of the control scheme, its rms magnitude deviates to less than 1% of the nominal value. In this scenario, the output voltage undershoot is less than 30.4% and the settling time (t_s) is about 1.2 ms. However, it is noted that the conventional SMC in Fig. 4(b) has a higher voltage undershoot of 55% and longer t_s of 2.4 ms compared to the proposed SMC in Fig. 4(a). It can be seen in Fig. 4(c) that the conventional PI-PI control scheme has a higher voltage undershoot of 64.5% and longer t_s of 2.85 ms compared to the proposed SMC. Next, the THDs for the proposed SMC in Fig. 4(a), the conventional SMC in Fig. 4(b), and the conventional PI−PI control scheme in Fig. 4(c) are 0.81%, 1.2%, and 1.53%, respectively. Hence, the low THD, small steady-state error (SSE), and robustness against parameter variations verify the better performance of the proposed SMC scheme compared to the conventional SMC scheme and the conventional PI−PI control scheme.

C. COMPARATIVE PERFORMANCE ANALYSIS UNDER AN UNBALANCED LOAD WITH WIDE-RANGE LC FILTER UNCERTAINTIES (i.e., 50% L_{f0} AND 150% C_{f0})

Next, the behavior of the proposed SMC in Fig. 5(a) is compared to that of the conventional SMC in Fig. 5(b) under the scenario of an unbalanced load with 50% L_{f0} and 150% C_{f0}. In this scenario, phase A is suddenly opened to observe the

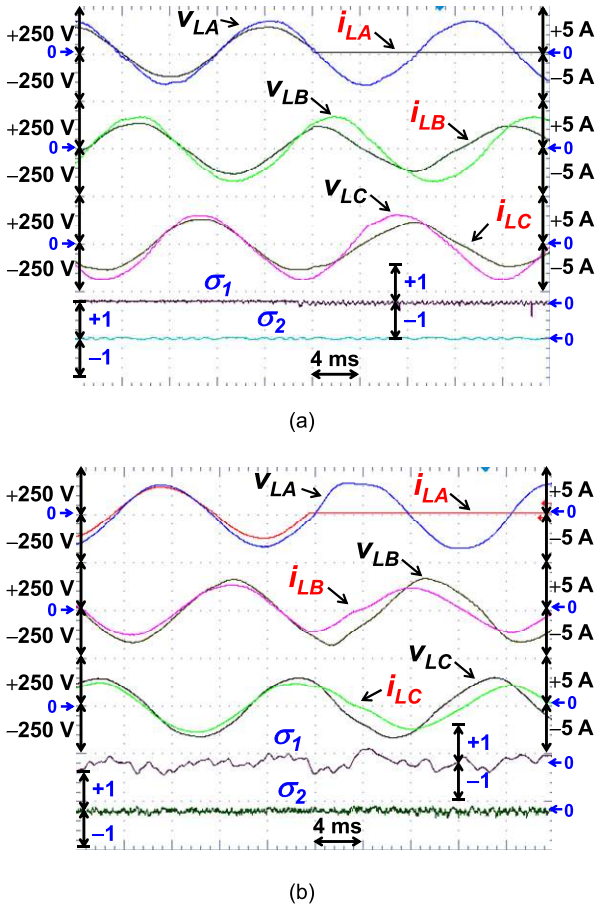

FIGURE 5. Experimental waveforms (v_L, i_L, σ_1, and σ_2) under an unbalanced load (i.e., suddenly phase A opened) with $L_f = 50\%\ L_{f0}$ and $C_f = 150\%\ C_{f0}$. (a) Proposed observer-based SMC scheme. (b) Conventional observer-based SMC scheme.

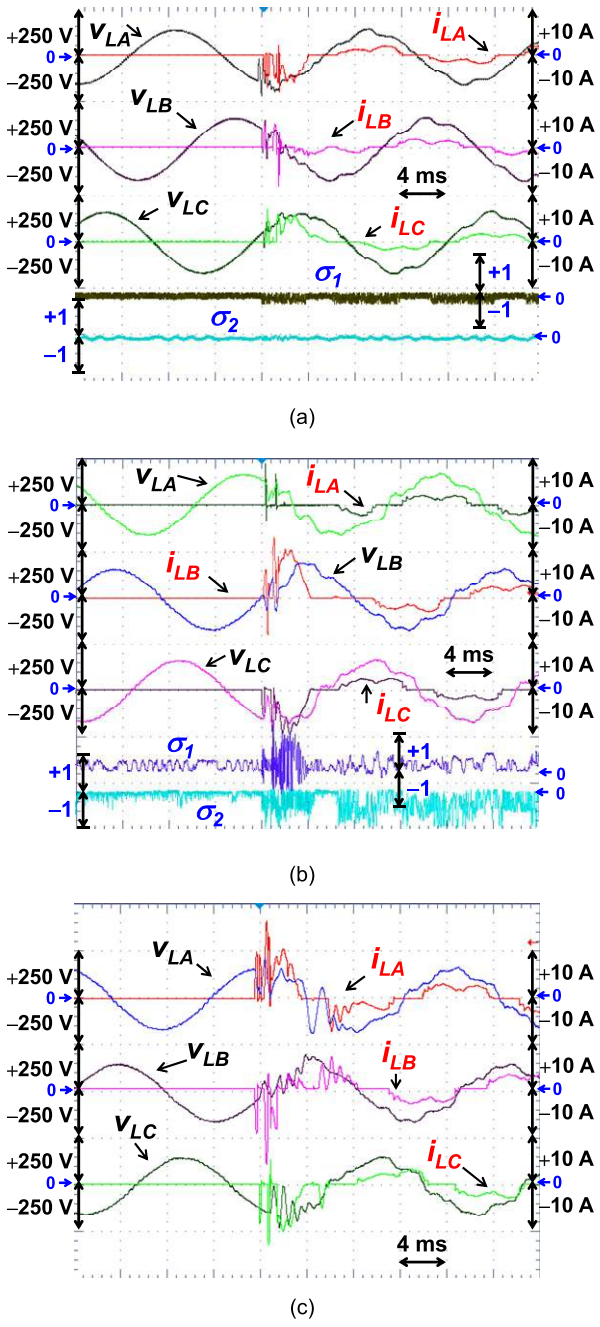

FIGURE 6. Experimental waveforms (v_L, i_L, σ_1, and σ_2) under a non-linear load step change (i.e., three-phase diode rectifier with crest factor of 2.15) with L_f = 150% L_{f0} and C_f = 150% C_{f0}. (a) Proposed observer-based SMC scheme. (b) Conventional observer-based SMC scheme. (c) Conventional PI−PI control scheme.

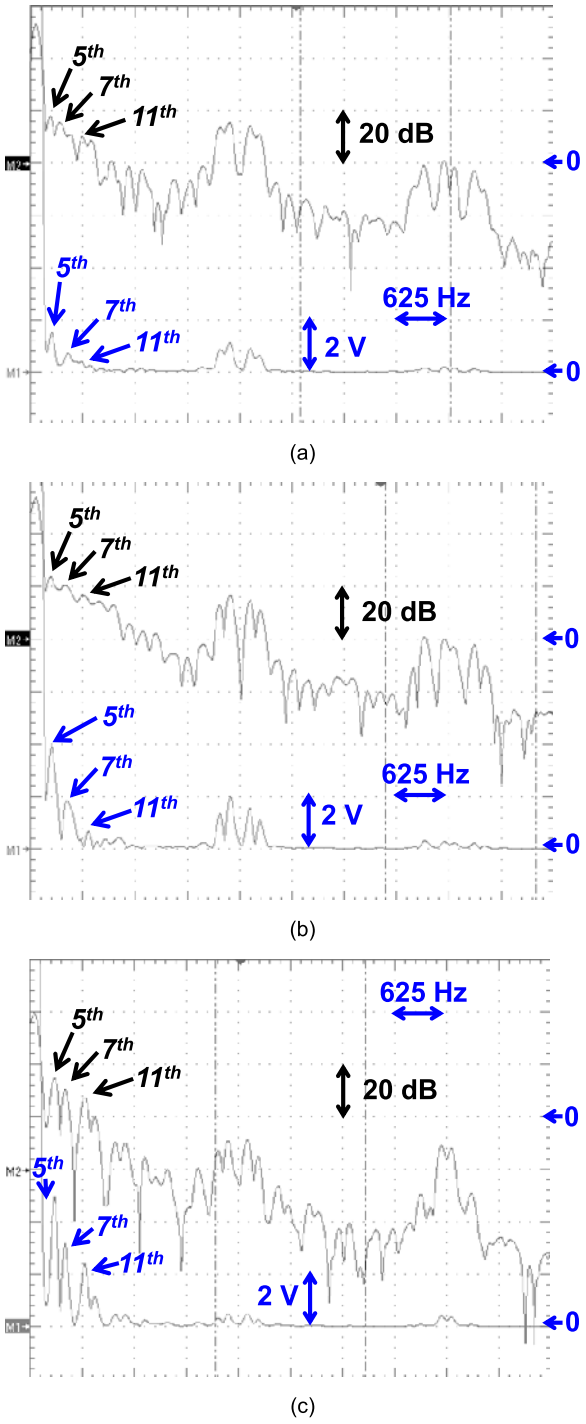

FIGURE 7. Experimental waveforms (Frequency spectrum of v_{La}) under a non-linear load (i.e., three-phase diode rectifier with crest factor of 2.15) with L_f = 150% L_{f0} and C_f = 150% C_{f0}. (a) Proposed observer-based SMC scheme. (b) Conventional observer-based SMC scheme. (c) Conventional PI−PI control scheme.

dynamic and steady-state behaviors of the proposed SMC and the conventional SMC. The waveforms of σ_1 and σ_2 verify that the proposed SMC can efficiently regulate the voltage under an unbalanced load condition due to the robust switching control law. Regardless of phase A opening, all output voltage waveforms in Fig. 5(a) are more sinusoidal than those in Fig. 5(b) because it is observed that the THDs/voltage dips in v_L for the proposed SMC and the conventional SMC are 0.85%/2% and 1.31%/4%, respectively.

D. COMPARATIVE PERFORMANCE ANALYSIS UNDER A SUDDEN NON-LINEAR LOAD STEP CHANGE WITH WIDE-RANGE LC FILTER UNCERTAINTIES (i.e., 150% L_{f0} AND 150% C_{f0})

Lastly, Fig. 6 illustrates the comparative performance analysis of the three control schemes (i.e., proposed SMC,

TABLE 2. Summary of the Comparative Performance Analysis of the Proposed SMC, Conventional SMC, and Conventional PI−PI.

Operating Schemes		THD [%]	t_s [ms]	Voltage Dip [%]	v_{LA} [V_{rms}]	v_{LB} [V_{rms}]	v_{LC} [V_{rms}]
1	Prop. SMC	0.81	1.2	30.4	109.8	109.7	109.8
	Conv. SMC	1.2	2.4	55	109.7	109.5	109.6
	Conv. PI–PI	1.53	2.85	64.5	108.5	108.1	108.4
2	Prop. SMC	0.85	-	2	109.7	109.7	109.8
	Conv. SMC	1.31	-	4	109.5	109.3	109.5
3	Prop. SMC	1.82	1.61	35.6	109.1	109.2	108.9
	Conv. SMC	3.38	3.5	67.1	107.9	108.1	107.8
	Conv. PI–PI	4.31	4.8	71.9	107.4	108.1	107.6

Note that "Prop." and "Conv." represents "proposed" and "conventional" respectively.

conventional SMC, conventional PI−PI) under the scenario of the sudden non-linear load step change (i.e., a three-phase diode rectifier shown in Fig. 3) with the 150% L_{f0} and 150% C_{f0}. It is noted that the non-linear load has the load resistor R_{load} while the capacitor C_{load} is pre-charged by the inverter. Because of the pre-charged capacitor voltage, the load current gets out of control for first one to two cycles during the transient-state after the insertion of the load resistor [3]. Fig. 6(a) highlights that the proposed SMC has a reduced THD (1.82%), faster t_s (1.61 ms), smaller output voltage undershoots (35.6%), and smaller SSE (1.5 V). Meanwhile, the experimental results of the conventional SMC (THD: 3.38%; t_s: 3.5 ms; voltage undershoot: 67.1%; SSE: 2.4 V) in Fig. 6(b) and the conventional PI-PI (THD: 4.31 %; t_s: 4.8 ms; voltage undershoot: 71.9%; SSE: 2.7 V) in Fig. 6(c) display higher THD, longer t_s, larger undershoot, and larger SSE compared to the proposed SMC. In addition, Fig. 6(a) shows that the output voltage is not almost affected despite the very high rate of change of the i_L. The sliding surfaces σ_1 and σ_2 under this scenario show small overshoots which are reflected in the v_L. Meanwhile, the higher perturbations in the v_L shown in Fig. 6(b) and (c) prove that the conventional SMC and conventional PI−PI control schemes are not effective to mitigate the wide range variations of an *LC* filter under a sudden non-linear load step change.

Next, Fig. 7 presents the frequency spectrum analysis of the load voltage in volts as well as dBs for the proposed SMC, conventional SMC, and conventional PI−PI, respectively. As depicted in Fig. 7(a), the magnitudes of 5^{th} (1.5 V) and 7^{th} (0.8 V) harmonic components for the proposed SMC are significantly reduced due to the relaxed conditions designed for the norm-bounds of the proposed SMC. The 5^{th} (3.99 V) and 7^{th} (1.92 V) harmonic components in Fig. 7(b) for the conventional SMC and 5^{th} (4.89 V) and 7^{th} (3.28 V) harmonic components in Fig. 7(c) for the conventional PI−PI are higher compared to the proposed SMC.

From the experimental results of the three scenarios, the proposed SMC method provided the better performance such as good voltage regulation and lower THDs compared to the conventional SMC method. Moreover, the proposed SMC showed more robustness against the wide range parameter uncertainties of L_f and C_f. Last, Table 2 presents a summary of the comparative performance analysis of the proposed SMC, conventional SMC, and conventional PI−PI under all three operating scenarios described previously.

VI. CONCLUSION

This paper presents an advanced sliding mode voltage controller to mitigate the matched and mismatched uncertainties of the *LC* filter in a three-phase voltage source inverter. The sliding surface is designed using the LMIs which can select the relaxed norm-bounded conditions for the matched and mismatched uncertainties. The sliding mode observer, due to its robustness to external disturbances, is also employed to estimate the load currents. The stability of the sliding mode dynamics and the reachability conditions are presented using the Lyapunov theory. The more robustness against *LC* filter uncertainties, lower THD, smaller steady-state error, and faster transient response of the proposed SMC were verified under the three scenarios of a sudden load change, an unbalanced load, and a sudden non-linear load change compared to the conventional SMC and conventional PI−PI control. The proposed SMC in this paper can be applied to various applications such as active power filter, STATCOM, and ac motor drive to compensate for matched and mismatched uncertainties.

REFERENCES

[1] M. Curkovic, K. Jezernik, and R. Horvat, "FPGA-based predictive sliding mode controller of a three-phase inverter," *IEEE Trans. Ind. Electron.*, vol. 60, no. 2, pp. 637–644, Feb. 2013.

[2] Z. Jian-Jian, C. Yong, C. Zhang-Yong, and Z. Anjian, "Open-switch fault diagnosis method in voltage-source inverters based on phase currents," *IEEE Access*, vol. 7, pp. 63619–63625, 2019.

[3] J. S. Lim, C. Park, J. Han, and Y. I. Lee, "Robust tracking control of a three-phase DC–AC inverter for UPS applications," *IEEE Trans. Ind. Electron.*, vol. 61, no. 8, pp. 4142–4151, Aug. 2014.

[4] F. D. Bosio, L. A. D. S. Ribeiro, F. D. Freijedo, M. Pastorelli, and J. M. Guerrero, "Effect of state feedback coupling and system delays on the transient performance of stand-alone VSI with LC output filter," *IEEE Trans. Ind. Electron.*, vol. 63, no. 8, pp. 4909–4918, Aug. 2016.

[5] H.-S. Kim and S.-K. Sul, "A novel filter design for output LC filters of PWM inverters," *J. Power Electron.*, vol. 11, no. 1, pp. 74–81, Jan. 2011.

[6] B. Guo, M. Su, Y. Sun, H. Wang, H. Dan, Z. Tang, and B. Cheng, "A robust second-order sliding mode control for single-phase photovoltaic grid-connected voltage source inverter," *IEEE Access*, vol. 7, pp. 53202–53212, 2019.

[7] J. Jo and H. Cha, "Design of effective passive damping resistor of grid-connected inverter with LCL filter for industrial applications," *J. Electr. Eng. Technol.*, vol. 14, no. 5, pp. 2039–2048, Sep. 2019.

[8] A. G. Yepes, F. D. Freijedo, O. Lopez, and J. Doval-Gandoy, "High-performance digital resonant controllers implemented with two integrators," *IEEE Trans. Power Electron.*, vol. 26, no. 2, pp. 563–576, Feb. 2011.

[9] E.-K. Kim, F. Mwasilu, H. H. Choi, and J.-W. Jung, "An observer-based optimal voltage control scheme for three-phase UPS systems," *IEEE Trans. Ind. Electron.*, vol. 62, no. 4, pp. 2073–2081, Apr. 2015.

[10] J. Rodriguez, M. P. Kazmierkowski, J. R. Espinoza, P. Zanchetta, H. Abu-Rub, H. A. Young, and C. A. Rojas, "State of the art of finite control set model predictive control in power electronics," *IEEE Trans. Ind. Informat.*, vol. 9, no. 2, pp. 1003–1016, May 2013.

[11] M. Nauman and A. Hasan, "Efficient implicit model-predictive control of a three-phase inverter with an output LC filter," *IEEE Trans. Power Electron.*, vol. 31, no. 9, pp. 6075–6078, Sep. 2016.
[12] D.-E. Kim and D.-C. Lee, "Feedback linearization control of three-phase UPS inverter systems," *IEEE Trans. Ind. Electron.*, vol. 57, no. 3, pp. 963–968, Mar. 2010.
[13] M. Kojima, K. Hirabayashi, Y. Kawabata, E. C. Ejiogu, and T. Kawabata, "Novel vector control system using deadbeat-controlled PWM inverter with output LC filter," *IEEE Trans. Ind. Appl.*, vol. 40, no. 1, pp. 162–169, Jan. 2004.
[14] T. D. Do, V. Q. Leu, Y.-S. Choi, H. H. Choi, and J.-W. Jung, "An adaptive voltage control strategy of three-phase inverter for stand-alone distributed generation systems," *IEEE Trans. Ind. Electron.*, vol. 60, no. 12, pp. 5660–5672, Dec. 2013.
[15] S. J. Chiang, T. L. Tai, and T. S. Lee, "Variable structure control of UPS inverters," *IEE Proc.-Electr. Power Appl.*, vol. 145, no. 6, pp. 559–567, 1998.
[16] A. Abrishamifar, A. Ahmad, and M. Mohamadian, "Fixed switching frequency sliding mode control for single-phase unipolar inverters," *IEEE Trans. Power Electron.*, vol. 27, no. 5, pp. 2507–2514, May 2012.
[17] S.-C. Tan, Y. M. Lai, C. K. Tse, and M. K. H. Cheung, "Adaptive feedforward and feedback control schemes for sliding mode controlled power converters," *IEEE Trans. Power Electron.*, vol. 21, no. 1, pp. 182–192, Jan. 2006.
[18] O. Kukrer, H. Komurcugil, and A. Doganalp, "A three-level hysteresis function approach to the sliding-mode control of single-phase UPS inverters," *IEEE Trans. Ind. Electron.*, vol. 56, no. 9, pp. 3477–3486, Sep. 2009.
[19] X. Hao, X. Yang, T. Liu, L. Huang, and W. Chen, "A sliding-mode controller with multiresonant sliding surface for single-phase grid-connected VSI with an LCL filter," *IEEE Trans. Power Electron.*, vol. 28, no. 5, pp. 2259–2268, May 2013.
[20] H. Komurcugil, "Rotating-sliding-line-based sliding-mode control for single-phase UPS inverters," *IEEE Trans. Ind. Electron.*, vol. 59, no. 10, pp. 3719–3726, Oct. 2012.
[21] Y. S. Choi, H. H. Choi, and J. W. Jung, "An adaptive sliding-mode control technique for three-phase UPS system with auto-tuning of switching gain," *Electr. Eng.*, vol. 96, no. 4, pp. 373–383, Dec. 2014.
[22] A. Houari, H. Renaudineau, J.-P. Martin, S. Pierfederici, and F. Meibody-Tabar, "Flatness-based control of three-phase inverter with output *LC* filter," *IEEE Trans. Ind. Electron.*, vol. 59, no. 7, pp. 2890–2897, Jul. 2012.
[23] J. Yang, S. Li, and X. Yu, "Sliding-mode control for systems with mismatched uncertainties via a disturbance observer," *IEEE Trans. Ind. Electron.*, vol. 60, no. 1, pp. 160–169, Jan. 2013.
[24] H. H. Choi, "LMI-based nonlinear fuzzy observer-controller design for uncertain MIMO nonlinear systems," *IEEE Trans. Fuzzy Syst.*, vol. 15, no. 5, pp. 956–971, Oct. 2007.
[25] S. Boyd, L. El Ghaoui, E. Feron, and V. Balakrishnan, *Linear Matrix Inequalities in System and Control Theory*. Philadelphia, PA, USA: SIAM, 1994.
[26] N. T.-T. Vu, D.-Y. Yu, H. H. Choi, and J.-W. Jung, "T–S fuzzy-model-based sliding-mode control for surface-mounted permanent-magnet synchronous motors considering uncertainties," *IEEE Trans. Ind. Electron.*, vol. 60, no. 10, pp. 4281–4291, Oct. 2013.
[27] B. Song and J. K. Hedrick, *Dynamic Surface Control of Uncertain Nonlinear Systems: An LMI Approach*. New York, NY, USA: Springer-Verlag, 2011.
[28] Y. Shtessel, C. Edwards, L. Fridman, and A. Levant, *Sliding Mode Control and Observation*. New York, NY, USA: Springer, 2014.
[29] D.-W. Chung, J.-S. Kim, and S.-K. Sul, "Unified voltage modulation technique for real-time three-phase power conversion," *IEEE Trans. Ind. Appl.*, vol. 34, no. 2, pp. 374–380, Mar./Apr. 1998.
[30] D. G. Holmes and T. A. Lipo, *Pulse Width Modulation for Power Converters: Principles and Practice*. Hoboken, NJ, USA: Wiley, 2003.

MUHAMMAD SAAD RAFAQ received the B.S. degree in electrical engineering from the University of Engineering and Technology, Taxila, Pakistan, in 2011, and the Ph.D. degree from the Division of Electronics and Electrical Engineering, Dongguk University, Seoul, South Korea, in 2019.

From 2012 to 2013, he was a Laboratory Engineer with the University of Gujrat, Gujrat, Pakistan. His research interests include distributed generation systems, control of power converters, parameter identification, electric vehicles, and DSP-based electric machine drives.

SADEQ ALI QASEM MOHAMMED received the B.S. degree in electrical engineering from Universiti Tun Hussein Onn Malaysia, Malaysia, in 2012, and the M.S. degree from the Division of Electrical and Information Engineering, Seoul National University of Science and Technology, Seoul, South Korea, in 2016. He is currently pursuing the Ph.D. degree with the Division of Electronics and Electrical Engineering, Dongguk University, Seoul.

From 2012 to 2013, he was a Research Assistant with Universiti Tun Hussein Onn Malaysia, Malaysia. His research interests include distributed generation systems, electric vehicles, and DSP-based electric machine drives.

HAN HO CHOI (Member, IEEE) received the B.S. degree in control and instrumentation engineering from Seoul National University, Seoul, South Korea, in 1988, and the M.S. and Ph.D. degrees in electrical engineering from the Korea Advanced Institute of Science and Technology, Daejeon, South Korea, in 1990 and 1994, respectively.

He is currently with the Division of Electronics and Electrical Engineering, Dongguk University, Seoul. His research interests include control theory and its applications to real-world problems.

JIN-WOO JUNG (Member, IEEE) received the B.S. and M.S. degrees in electrical engineering from Hanyang University, Seoul, South Korea, in 1991 and 1997, respectively, and the Ph.D. degree in electrical and computer engineering from The Ohio State University, Columbus, OH, USA, in 2005.

From 1997 to 2000, he was with the Home Appliance Research Laboratory, LG Electronics Company, Ltd., Seoul. From 2005 to 2008, he was a Senior Engineer with the Research and Development Center, PDP Development Team, Samsung SDI Company Ltd., South Korea. Since 2008, he has been a Professor with the Division of Electronics and Electrical Engineering, Dongguk University, Seoul. His research interests include DSP-based electric machine drives, distributed generation systems using renewable energy sources, and power conversion systems and drives for electric vehicles.